



Preparation, characterization and thermal properties of dodecanol, palmitic acid and hydroxylpropyl methyl cellulose as novel form-stable phase change materials

Meijie Qu^{1,2} · Chuigen Guo¹ · Liping Li¹

Received: 22 July 2020 / Accepted: 19 May 2021 / Published online: 20 June 2021
© Akadémiai Kiadó, Budapest, Hungary 2021

Abstract

In order to adjust buildings temperature, a dodecanol (DD)-palmitic acid (PA)/hydroxylpropyl methyl cellulose (HPMC) composite phase change material was prepared by vacuum impregnation. DD-PA was absorbed into the HPMC, which was verified by specific surface area, pore size (BET) and scanning electron microscopy (SEM) analysis. The results of Fourier transform infrared spectroscopy (FTIR) and X-ray diffractometer (XRD) indicated that the HPMC and DD-PA were only physical combination. The differential scanning calorimetry (DSC) analysis revealed that the phase change temperature and latent heat were 19.34 °C and 113.12 J g⁻¹, which means good energy storage capacity. The 5% mass loss temperatures ($T_{.5\%}$) of thermo-gravimetric analysis (TG) was higher than 50 °C, showing the good thermal stability of composite phase change materials. About 60% DD-PA was absorbed in HPMC, which detected by DSC and TG. After 100 thermal cycling, the latent heat, onset temperature (T_0), peak temperature (T_{peak}) and end temperature (T_{end}) had changed -1.02%, -8.20%, -4.29% and -5.60%. The result showed that the composite phase change materials own good thermal reliability. In addition, the 2% multi-walled carbon nanotubes (MW CNTs) were added to improve the thermal conductivity. And the thermal conductivity was increased from 0.130 to 0.172 W (mK)⁻¹, the total thermal storage-release time was decreased from 3740 to 2310 s.

Keywords Eutectic mixture · Thermal conductivity · Multi-walled carbon nanotubes · Phase change materials

Introduction

Thermal energy storage (TES) was attracting more and more attention for its widely application in energy conservation, utilization of renewable energy resources and ability to deal with the discrepancy between the energy demands and supply [1–4]. TES was composed of sensible heat, latent heat and thermo-chemical reaction heat [5]. Latent heat thermal energy storage (LHTES) was also taken as phase change energy storage, the most attractive method in TES. In LHTES method, energy was stored in phase change

materials (PCM) in the shape of latent heat [6]. PCM can absorb or release quantity of latent energy in the phase change process and keep the outer temperature at a relatively constant level [7–9]. There are many advantages in LHTES, such as high-energy storage density, suitable and broad phase change temperature ranges, stable chemical structure, and low-cost [10–12]. Thus, the application of LHTES was comprehensive, such as buildings [13], heating and cooling [14], textile [15], greenhouse [16], thermal insulation [17], and food or medicine conserving [18, 19].

The PCM was usually divided into two types: organic PCM and inorganic PCM. The organic PCM such as paraffin, PEG, fatty acids and fatty alcohols owns superior properties than inorganic PCM such as water, salt hydrates, salt solutions, and metals [20]. These superior properties contain low-cost, little or no super-cooling, no phase segregation [21–23]. The super-cooling and phase segregation particularly impact on the energy storage capacity. For these superior properties, the fatty acids, and fatty alcohols could be used into different compartments of buildings such as wallboards [24], walls [25], floors and ceilings [26]. But the

✉ Liping Li
lilipingguo@126.com

¹ Key Laboratory for Biobased Materials and Energy of Ministry of Education, College of Materials and Energy, South China Agricultural University, 483 Wushan Road, Guangzhou 510642, China

² Department of Polymer Material and Engineering, School of Chemical Engineering, Dalian University of Technology, Dalian 116024, China

fatty acids, and fatty alcohols could not be directly used in buildings for the following two aspects: the seepage in the phase transition process and the low thermal conductivity [27]. Palmitic acid (PA), as a fatty acid, could not be directly used in buildings not only because of the above two aspects, but also for its high melting temperature (62 °C). In order to use the PA in buildings, binary or ternary eutectic mixtures were made instead of single PA. Dodecanol (DD) mixed with PA to form the eutectic mixture. And in this way, the phase change temperature could be largely decreased. Rohitash Kumar et al. tested the thermal properties of the palmitic acid and dodecanol eutectic mixtures. The results showed that the melting temperature was 20.08 °C, lower than the melting temperature of PA [28]. Though the high phase change temperature of PA had been solved, but the solution of the seepage and the low thermal conductivity had not been mentioned in their study.

Microencapsulation, melt blending and absorption technique were frequently used to prevent the seepage of PCM. Yeliz Konuklu et al. had used melamine-urea-formaldehyde resin as wall and capric acid as core, to fabricate the composite PCM without leakage according to situ polymerization technique [29]. Huang et al. applied melt blending method, based on fatty acid as PCM, HDPE-EVA as supporting materials, and no leakage was discovered [30]. Yang et al. used porous absorption method to prepare myristic-palmitic-stearic acid/expanded graphite composites and found there was no seepage during the phase transition process [31].

Porous absorption method was selected because it is the cheapest and simplest method to preventing PCM from seepage. Hydroxylpropyl methyl cellulose (HPMC) is one of the cellulose derivatives which derived from the natural cellulose or bacteria. HPMC was chosen as adsorption materials in this study because of its porosity, low price and large surface area. But HPMC owns low thermal conductivity, low thermal conductivity caused the little response rate to surrounding temperature. At the same time, various problems also appear such as insufficient energy storage and low energy storage efficiency. So, the thermal conductivity must be improved.

To solve the low thermal conductivity, many researchers had added expanded graphite, expanded perlite, metal and carbon nanotubes into PCMs [32]. Patrik Sobolciak et al. found only 15% expanded graphite could largely improve the thermal conductivity of LLDPE/wax [33]. Zhang et al. used carbon nanotubes to enhance the thermal conductivity of palmitic-stearic acid binary eutectic mixture. And 5% carbon nanotubes increased the thermal conductivity about 20.2% [34].

Multi-walled carbon nanotubes (MW CNTs), as nanomaterials with less dense and high thermal conductivity, had shown superior applications to enhance the thermal conductivity of phase change materials [35]. It was used in this

paper for its higher thermal conductivity, better compatibility, lower density than other thermal conductivity enhancer. Xu et al. used MW CNTs as the thermal conductivity additive of paraffin/diatomite, only 0.26% MW CNTs, the thermal conductivity increased 42.45% [36].

The main purpose of this study was to develop a PA composite PCM with no leakage, high thermal conductivity and suitable phase change temperature for use in buildings. The solution of the leakage of DD-PA had not been reported. In this paper, the DD-PA eutectic mixture was prepared to reduce the phase change temperature of PA. DD-PA eutectic mixture was absorbed into HPMC to prevent seepage. Then MW CNTs were appended to improve the thermal conductivity of the DD-PA/HPMC. The thermal conductivity ability was checked by the thermal conductivity and thermal storage/release rate. The phase transition temperature and latent heat were checked by DSC. The thermal stability and thermal reliability were studied by TG and thermal cycling test. The chemical interaction was analyzed by FTIR and XRD.

Materials and experimental methods

Materials

Hydroxylpropyl methyl cellulose (HPMC) was obtained from Yanxing Chemical Engineering Co., Ltd (Hebei, China). Palmitic acid (PA) and dodecanol (DD) were acquired from Fuchen Chemical Reagent Co., Ltd (Tianjin, China). Multi-walled carbon nanotubes (MW CNTs) were got from Beijing Deke Island Gold Technology Co., Ltd. (Beijing, China), outside diameter: 10–20 nm, length: 10–30 μm.

Synthesis of DD-PA/HPMC phase change material

Synthesis of DD-PA eutectic mixture

PA and DD can be intermingled with each other to form the eutectic mixture to accomplish the eutectic temperature, according to the lowest eutectic point theory. Eutectic temperature is far below than the individual component melting temperature. The eutectic proportion could be figured up with Schrader Eq. (1).

$$T = 1 / (1/T_f - RT \ln X_A / \Delta_s^1 H_A) \quad (1)$$

T presents the eutectic mixture temperature, namely the phase change temperature of the eutectic mixture. X_A is on behalf of the mass percentage of component DD in the eutectic mixture. $\Delta_s^1 H_A$ and T_f are the fusion latent heat and

melting temperature of component DD. R is the gas constant $8.314 \text{ J K}^{-1} \text{ mol}^{-1}$.

In this study, the DD and PA have melting temperature of $24.00 \text{ }^\circ\text{C}$ and $62.00 \text{ }^\circ\text{C}$, fusion latent heat of 186.00 J g^{-1} and 208.00 J g^{-1} , respectively. The calculated ratio of DD-PA was $89.60/10.40$, and the lowest eutectic temperature was $22.19 \text{ }^\circ\text{C}$.

DD and PA were weighed up as the above calculated ratio and heated at $70 \text{ }^\circ\text{C}$ until DD and PA completely melt in an Erlenmeyer flask. Then the Erlenmeyer flask was transferred to an ultrasonic cleaner for 2 h to make DD and PA completely dispersion. The eutectic mixture was obtained.

Synthesis of DD-PA/HPMC phase change materials

50 g HPMC was dried at $80 \text{ }^\circ\text{C}$ for 8 h. Fifty grams of HPMC was placed in a 500 mL filter flask firstly, and then 200 mL DD-PA was added in the filter flask. The filter flask was transferred to the ultrasonic cleaner, which made the HPMC to absorb DD-PA adequately. Then a rubber stopper was put on the neck of the filter flask, and the filter flask was vacuumed at 50 kPa for 90 min; then, the rubber stopper was taken away and the vacuum pump was turned off for 40 min. In this way, the DD-PA was forced in the pore of the HPMC. Finally, the sample was heated in a dryer at $80 \text{ }^\circ\text{C}$ for 24 h, and the purpose was to get rid of the residual DD-PA on the surface of HPMC.

Synthesis of DD-PA/HPMC/MW CNTs phase change materials

1 g MW CNTs (2 mass% of HPMC) were added, and above step was repeated. The DD-PA/HPMC/MW CNTs were got, and the preparation process is shown in Fig. 1. Both cellulose and MW CNTs can adsorb DD-PA. After fully dispersed, DD-PA/HPMA/MW CNTs were dispersed evenly, thus showing a uniform distribution in Fig. 1.

Characterization

Brunauer–Emmett–Teller (BET)

BET method was used to characterize the pore structure of HPMC and DD-PA/HPMC. The surface areas of samples were determined by specific surface analysis (JW-BK132, JW, China) after samples vacuum-dried at $80 \text{ }^\circ\text{C}$ for 12 h. The nitrogen adsorption–desorption isotherms curve was measured with the sample temperature $-196.15 \text{ }^\circ\text{C}$ and the pressure (P/P_0) between 10^{-6} and 1. The pore size distribution was counted using Barrett–Joyner–Halenda (BJH) method for the adsorption curve.

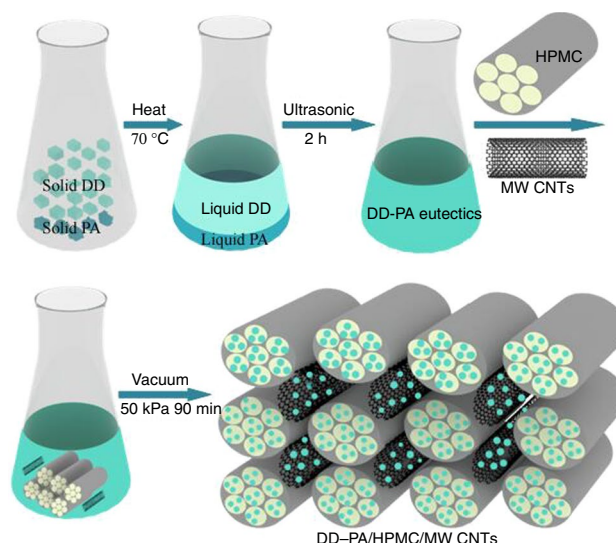


Fig. 1 Preparation process of DD-PA/HPMC/MW CNTs

Fourier transform infrared (FTIR) spectrophotometer

Fourier transform infrared (FTIR) spectrophotometer (Spectrum 100, Perkin-Elmer, America) was used to check the chemical structures of DD, PA, DD-PA, HPMC, uncycled DD-PA/HPMC and DD-PA/HPMC after 100 times cycle. The FTIR spectrum of $400\text{--}4000 \text{ cm}^{-1}$ was recorded with a resolution of 4 cm^{-1} .

X-ray diffractometer (XRD)

The crystalloid phases of DD-PA, HPMC and DD-PA/HPMC were measured using the X-ray diffractometer (XRD, Bruker D8 Advance, AXs, Bruker, Germany). The curves of XRD were obtained with Ni-filtered $\text{CuK}\alpha$ ($\lambda = 0.15406 \text{ nm}$) radiation with a continuous scanning speed of $5 \text{ }^\circ/\text{min}$.

Scanning electron microscopy (SEM)

Scanning electronic microscope (SEM) was used to observe the surface morphology of HPMC and DD-PA/HPMC. The SEM images were taken by JEOL JSM-7500F SEM (JEOL, Japan). The SEM samples were plated with platinum before the observation.

Differential scanning calorimeter (DSC)

Differential scanning calorimeter (DSC, Pyris Diamond, Perkin-Elmer, America) was measured the melting, freezing temperature and latent heat of uncycled DD-PA/HPMC and DD-PA/HPMC after 100 cycling times. The samples

(3–5 mg) were positioned in an aluminum crucible. Then the samples were heated from room temperature to 200 °C (maintain 5 min at 200 °C) at a rate of 50 °C min⁻¹, in terms of eliminating thermal history. The thermal storage properties were detected from 0 °C to 90 °C at a rate of 5 °C min⁻¹.

Thermal cycling test

The thermal cycling test was studied the thermal reliability of the DD-PA/HPMC during melting and freezing process. The test had been performed continuously for 100 times in the range of -10 to 90 °C. The probable changes in thermal and chemical were investigated by DSC and FTIR analyses.

Thermo-gravimetric analysis (TG)

The TG (Pyris 1, Perkin-Elmer, America) was used to measure the thermal stability of phase change materials. The samples (3–5 mg) were heated from room temperature to 600 °C under nitrogen atmosphere at a rate of 10 °C min⁻¹.

Thermal conductivity test

The thermal conductivity was detected by Hot-disk Thermal Constant Analyzer (TPS 2500 s, Hot Disk AB Company, Sweden). The samples were measured three times at room temperature and took the average to eradicate any discrepancies.

The thermal storage-release test

The glass tube containing 10 g samples was placed into a water basin. The samples were heated from 10 to 60 °C and then cooled from 60 to 10 °C. The temperature was recorded by a multi-channel temperature recorder.

Results and discussion

Pore structure of DD-PA/HPMC and HPMC

BET method was carried out to obtain the pore diameter distribution curves and N₂ adsorption–desorption curves, to check the change of pore state and absorption of HPMC.

Figure 2 shows the pore diameter distribution curves of DD-PA/HPMC and HPMC. Double peaks curves were presented in the pore diameter distribution curves of HPMC. The peaks were 2.49 and 13.90 nm. The pore diameter distribution curves changed to triple-peaks curves in DD-PA/

HPMC, and the peaks were 1.69, 4.91, 12.30 nm. From these, it is easy to find that the pore diameter distribution of DD-PA/HPMC was decreased a lot. In this way, the pore of HPMC was decreased or even disappeared. Thereby, this result showed that the DD-PA eutectic mixture was absorbed into HPMC, and the pore structure of HPMC changed. On the other hand, the vertical coordinates presented the mass percentage of corresponding peak, and the mass ratios of the peaks for HPMC were all decreased which showed that the pore ratio was decreased. So, this result showed that the DD-PA eutectics were absorbed into HPMC again.

Figure 3 presents the N₂ adsorption–desorption curve of HPMC and DD-PA/HPMC. From Fig. 3, the HPMC was II type isotherms curve. The adsorption rate rose rapidly when the P/P_0 in a low region, and this indicated that the interaction between HPMC and N₂ was higher than N₂ to N₂. But the isotherm inflection point was showed at B point, and monolayer adsorption was formed in this time. However, with the pressure rising, the curve rose rapidly again for the monolayer adsorption formed [37].

The curve of DD-PA/HPMC was III type isotherm. This was typical BET multi-molecular layer adsorption curve and the DD-PA/HPMC pore was open-ended tubular capillary [38]. Under low pressure, there was small adsorption capacity for the interaction between DD-PA/HPMC and N₂ was very weak; on the contrary, the interaction between N₂ and N₂ was relatively strong. This result showed that the DD-PA eutectic mixture had been adsorbed in the pore of HPMC and the pore structure of HPMC had been changed. But when at high pressure, the adsorption–desorption go up very fast. For only a little adsorption of N₂, the adsorption of N₂ would emerge auto acceleration, and the number of adsorption layers is no longer limited.

HPMC has large specific surface area and favorable adsorption ability because of its porous fiber structure. The total pore volume of HPMC was 0.00419 cm³ g⁻¹, and the specific surface area of HPMC was 3.106 m² g⁻¹. This result

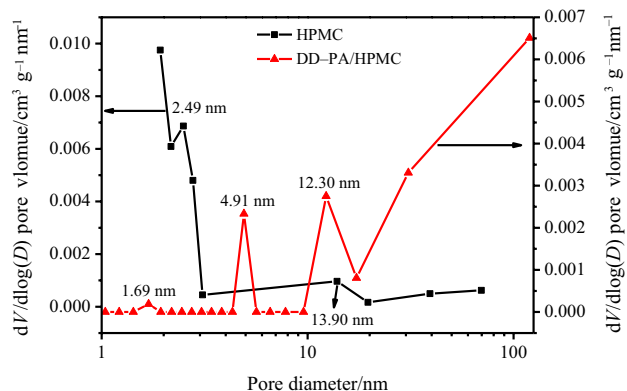


Fig. 2 Pore diameter distribution of HPMC and DD-PA/HPMC

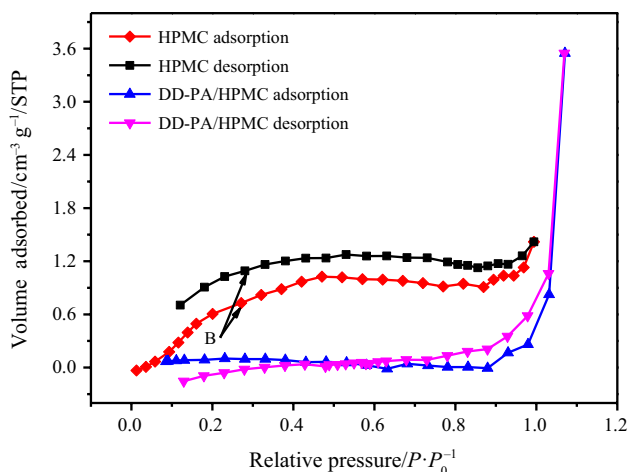


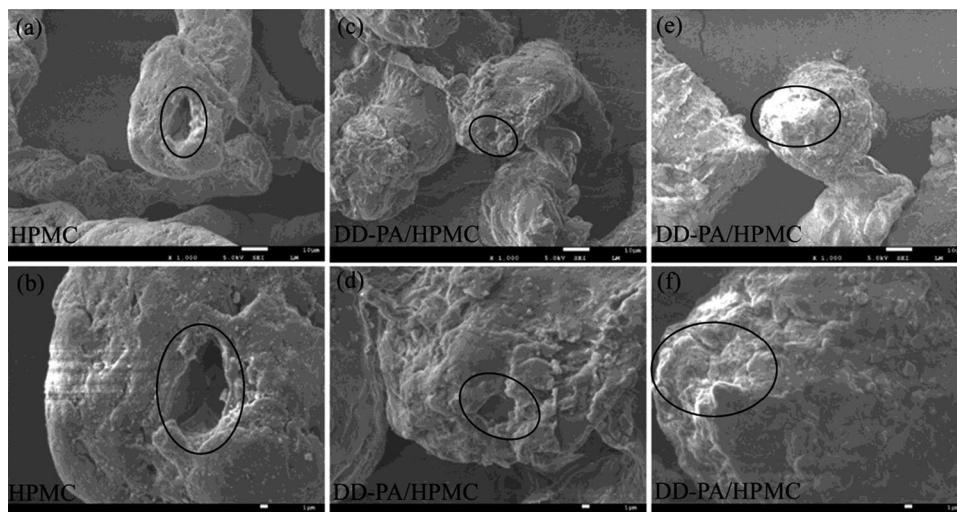
Fig. 3 N_2 adsorption–desorption curve of HPMC and DD-PA/HPMC

showed the good adsorption ability and high specific surface area of HPMC. However, the total pore volume of DD-PA/HPMC was $0.00249 \text{ cm}^3 \text{ g}^{-1}$ and the specific surface area of DD-PA/HPMC was $0.265 \text{ m}^2 \text{ g}^{-1}$. The specific surface area and total pore volume changed from 3.106 to $0.265 \text{ m}^2 \text{ g}^{-1}$ and from 0.00419 to $0.00249 \text{ cm}^3 \text{ g}^{-1}$, respectively. Consequently, it proved that the DD-PA eutectic mixture had been absorbed into HPMC. The result was fit with the results of pore size distribution and N_2 adsorption–desorption curve.

Microstructure of DD-PA/HPMC composite

Figure 4 displays the morphologies of HPMC and DD-PA/HPMC. But the SEM image of DD-PA was not got, for the DD-PA was melt when the electron beam focused on it. The SEM images of HPMC in Fig. 4a, b showed that HPMC has

Fig. 4 SEM images of HPMC and DD-PA/HPMC



a long fibrous structure and a porous rough surface which increased the specific surface area of HPMC. Therefore, the absorption rate of DD-PA was very high. In Fig. 4c–f, it is easy to find that the porosity was decreased and the surface was rougher. In brief, the SEM image of DD-PA/HPMC indicated that the DD-PA distributed evenly in the holes and surface of HPMC. This result meets the result in BET.

Chemical compatibility and interaction between HPMC and DD-PA/HPMC

FTIR and XRD measured the components of composite DD-PA/HPMC, in terms of studying the chemical compatibility and interaction. Figure 5 displays the characteristic peaks transmittance spectra of DD, PA, DD-PA, HPMC and DD-PA/HPMC. In the pure PA spectrogram, the peaks at 2929.70 cm^{-1} , 2828.38 cm^{-1} and 1469.49 cm^{-1} were the symmetrical stretching vibration and bending vibration peaks of $-\text{CH}_2$. The peak at 721.25 cm^{-1} represented the in-plane rocking vibration of $-\text{CH}_2$ group. Similarly, the above characteristic peaks were also existed in DD. The peak at 1700.91 cm^{-1} corresponded to the $-\text{COOH}$ stretching vibration.

In the spectrogram of DD, the peak at 3357.46 cm^{-1} was given rise to the $-\text{OH}$ stretching vibration. The peak recorded at about 1043.30 cm^{-1} ascribed to the $\text{C}-\text{O}$ stretching band.

Besides, in the spectra of HPMC, the peak at 1116.58 cm^{-1} was contributed by the $\text{C}-\text{O}-\text{C}$ stretching vibration.

Contrast to the FTIR spectrogram of PA and DD, DD-PA, HPMC and DD-PA/HPMC, it was easy to found that the spectrogram of DD-PA, DD-PA/HPMC contained all the peaks of PA and DD, DD-PA and HPMC and there was no new characteristic peak. The FTIR spectrum proved that the

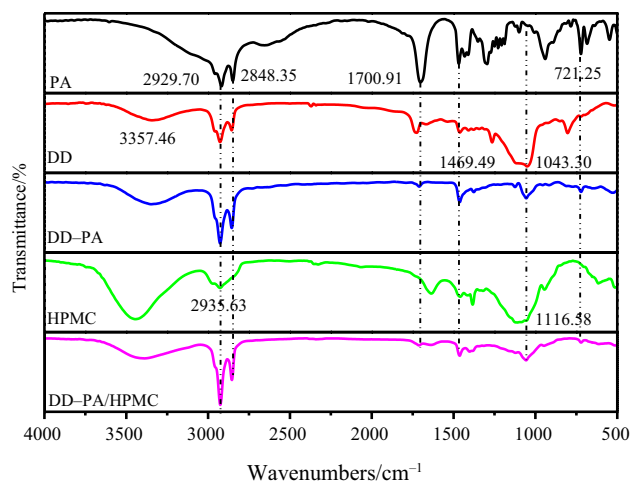


Fig. 5 FTIR spectra of PA, DD, DD-PA, HPMC and DD-PA/HPMC

reaction was physical. The only difference is some slight peaks shift and peaks weaken. This indicated there are some interactions between the $-OH$ of the DD and the $-COOH$ of the PA, the $-COOH$ of eutectics and the alkaline region of HPMC, which could prevent the seepage from the pores of HPMC when the temperature is above the fusing point.

Figure 6 displays the XRD curves of DD-PA, HPMC and DD-PA/HPMC. The peak at $2\theta = 20.50^\circ$ was the main peak of HPMC. The DD-PA eutectic mixture was regular crystallized with peaks at 18.06° , 19.84° , 23.26° and 24.42° while the peaks were at 19.02° , 21.49° and 23.83° in DD-PA/HPMC curve. Therefore, DD-PA/HPMC possesses similar crystalline texture and crystal cell type with DD-PA. It further confirmed that there was no chemical reaction between DD-PA and HPMC, which was accorded with the FTIR result.

Thermal properties of DD-PA and DD-PA/HPMC

DSC conducted the thermal storage properties of DD-PA and DD-PA/HPMC, such as phase change temperature and latent heat. Figure 7 shows the melting and solidification DSC curves of DD-PA eutectic mixture and DD-PA/HPMC, Table 1 summarizes the phase change parameters calculated from DSC curves.

From Fig. 7 and Table 1, the melting and solidifying peak phase change temperature was measured as 24.33°C and 15.78°C in the DD-PA curves, much lower than individual phase change materials DD and PA. And the melting and solidifying latent heat of DD-PA was 189.85 J g^{-1} and 157.32 J g^{-1} . The above results showed that the DD largely decreased the phase change temperature of PA. So, the PA was promising for buildings on account of the appropriate

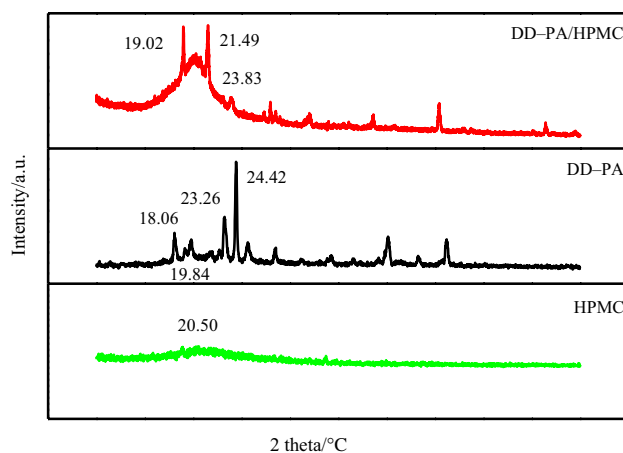


Fig. 6 XRD curves of DD-PA/HPMC, DD-PA and HPMC

phase change temperature and high latent heat. Thankfully, after PA was absorbed into HPMC, it could be used directly in buildings.

From Table 1, it showed that the T_0 , T_{peak} and T_{end} values of DD-PA/HPMC were 0.08 – 1.27°C lower than DD-PA eutectic mixture. These results were agreed with the reported by Radhakrishnan and Gubbins [39]. In their studies, they found that the slight shift of temperature values was because of the slight attractive interaction between the fluid and the hole surface. Likewise, in this paper, the depressed phase change temperature was caused by the slight interaction between the liquid DD-PA and the hole of HPMC.

From Table 1, the melting latent heat was measured as 113.12 J g^{-1} for DD-PA/HPMC. The DD-PA percentage was counted with 59.58%. Through the data of Table 1, it could be found that the thermal properties of DD-PA/HPMC were similar to the DD-PA. Luckily, that means DD-PA/HPMC was a good phase change material which could be used in building energy conversion.

Thermal reliability of DD-PA/HPMC

It is well known that a perfect PCM should not only have superior heat storage ability, but also should have very little change in thermal and chemical properties after long-term use. This ability was conducted by cycling test. DSC was carried out to detect the change of the thermal properties before and after 100 times cycling. The results were shown in Fig. 8, and the data from Fig. 8 were presented in Table 1.

The latent heat had changed -1.02% for DD-PA/HPMC, and the T_0 , T_{peak} and T_{end} had changed -8.20% , -4.29% , -5.60% for DD-PA/HPMC, respectively. The little changes were acceptable. It can also be concluded that the DD-PA/HPMC owns a favorable thermal reliability.

Fig. 7 Melting (a) and solidifying (b) DSC curves of DD-PA and DD-PA/HPMC

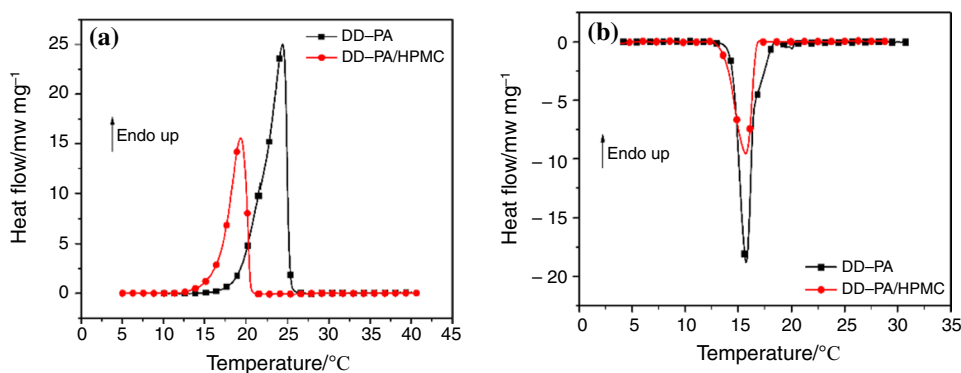


Table 1 The phase change parameters calculated from DSC

Samples	$T_0/^\circ\text{C}$	$T_{\text{peak}}/^\circ\text{C}$	$T_{\text{end}}/^\circ\text{C}$	Latent heat/ J g^{-1}	
Melting	DD-PA	15.05	24.33	25.84	189.85
	DD-PA/HPMC	11.34	19.34	20.91	113.12
Solidifying	DD-PA	13.61	15.78	18.35	157.32
	DD-PA/HPMC	12.50	15.92	17.04	94.47
DD-PA/HPMC after 100 times cycle	10.41	18.51	19.74	111.96	

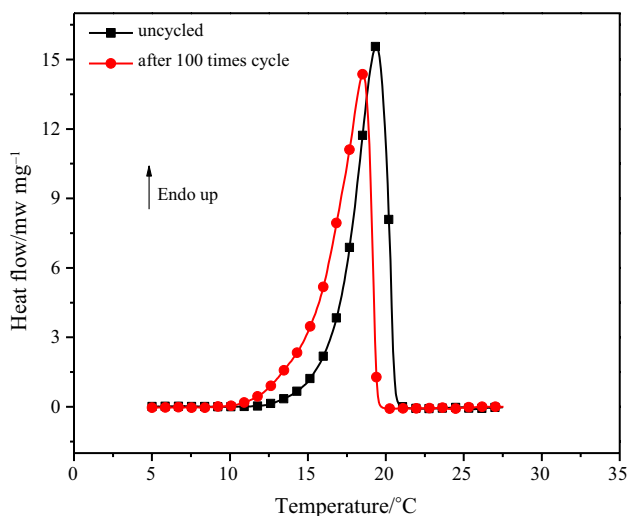


Fig. 8 DSC curve of uncycled and after 100 times cycle DD-PA/HPMC

From cycling test, there was little change on thermal properties, and it also be concluded that there was no seepage.

In addition, Fig. 9 shows the FTIR spectrums of uncycled and after 100 times cycle DD-PA/HPMC. There were no essential changes in the outline and wavenumbers before and after 100 times cycle. These results exhibited there was no decomposition in the chemical. The little change of latent heat was caused by the repeated cycling. The changes were only caused by the certain amounts of DD-PA. Accordingly, it could be concluded that the

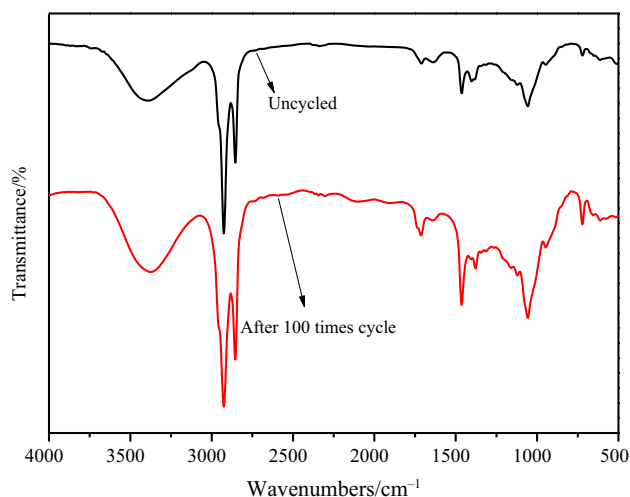


Fig. 9 FTIR spectra of uncycled and after 100 times cycle DD-PA/HPMC

DD-PA/HPMC composite phase change material was stable in chemical and thermal after 100 times cycle.

Thermal stability of DD-PA/HPMC

It is significant to evaluate the thermal stability of DD-PA/HPMC. TG was usually carried out to assess the thermal stability. Figure 10 exhibits the TG curves of DD-PA, HPMC and DD-PA/HPMC. The DD-PA/HPMC, DD-PA and HPMC 5% mass loss temperatures ($T_{-5\%}$) were 131.1

°C, 128.9 °C and 337.8 °C. The $T_{.5\%}$ was largely higher than 50 °C (the maximum temperature used in construction buildings). So, the thermal stability was enough using in buildings. The DD-PA and HPMC had only one degradation peak, and the degradation ranges of DD-PA and HPMC were 90–270 °C and 280–420 °C. However, the DD-PA/HPMC degraded in two processes. The first process was corresponding to the degradation of the DD-PA (about 60%), and the second process was HPMC (< 40%), which included some char residue of HPMC. This value was agreed with DSC.

Thermal conductivity of DD-PA/HPMC

The heat storage efficiency, depending on the thermal conductivity, was vital to select energy storage material. Thus, 2% MW CNTs were added to increase the thermal conductivity of the prepared DD-PA/HPMC.

Figure 11 showed the thermal conductivity results of DD-PA, DD-PA/HPMC and DD-PA/HPMC/MW CNTs. The conductivity declined 13.90% with the additive of HPMC. But when 2% MW CNTs were added into DD-PA/HPMC, the conductivity improved 32.30%. The thermal conductivity was enhanced largely with the additive of MW CNTs. For MW CNTs own a very large aspect ratio, so the heat exchange performance is very high. Only a small amount of MW CNTs doped in the composites, the thermal conductivity will be greatly improved [40].

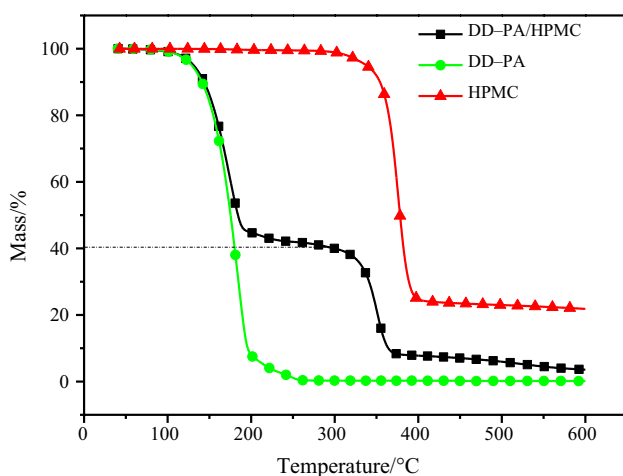


Fig. 10 TG curves of DD-PA, HPMC and DD-PA/HPMC

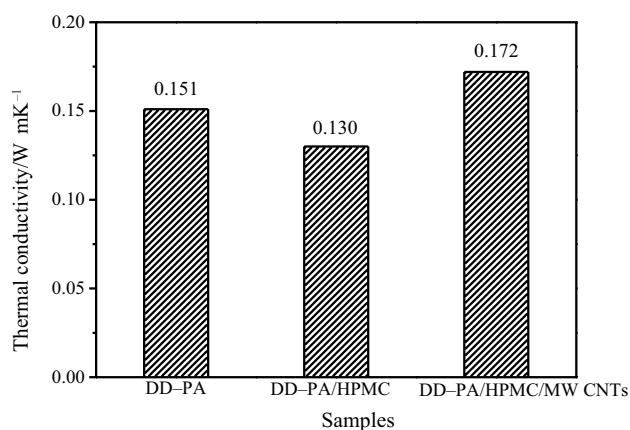


Fig. 11 Thermal conductivity of DD-PA, DD-PA/HPMC and DD-PA/HPMC/MW CNTs

The thermal storage-release characteristics of DD-PA/HPMC

The enhanced thermal conductivity was also checked by the thermal storage, thermal release and the total times of DD-PA, DD-PA/HPMC and DD-PA/HPMC/MW CNTs. Figure 12 shows the thermal storage-release curves of DD-PA, DD-PA/HPMC and DD-PA/HPMC/MW CNTs. From Fig. 12, the thermal storage times were 1340 s, 1660 s and 720 s for DD-PA, DD-PA/HPMC and DD-PA/HPMC/MW CNTs. The thermal release times were 1930 s, 2080 s and 1590 s and the total times were 3270 s, 3740 s and 2310 s. From the data, DD-PA/HPMC/MW CNTs had the fastest thermal storage and release rate, and DD-PA/HPMC was the slowest. Namely, DD-PA/HPMC/MW CNTs had the highest thermal conductivity and can transfer heat rapidly. The results meet the result of the thermal conductivity. In

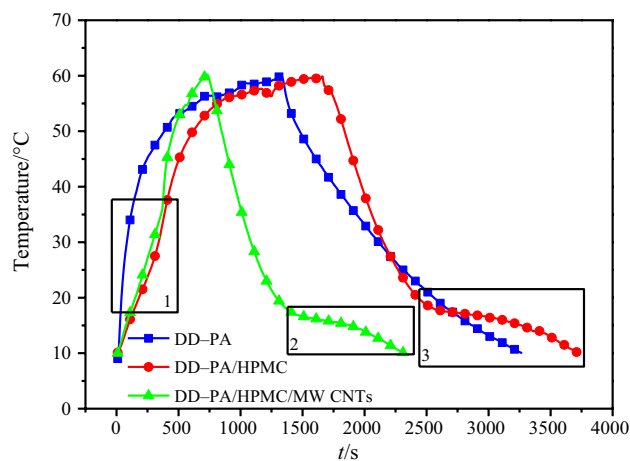


Fig. 12 Melting and freezing performance curves of DD-PA, DD-PA/HPMC and DD-PA/HPMC/MW CNTs

Fig. 12 region 1, the temperature increased slower than the other temperature ranges, for the heat absorption of melting endothermic. But in region 2 and region 3, the temperature decreased slower than the other temperature ranges, for the heat release of solidification.

Conclusions

In this study, a DD-PA/HPMC was made by vacuum adsorption for the further application of thermal storage. The DD-PA eutectic was firstly prepared with the ratio of 89.60:10.40 base on the theoretical calculation. HPMC, a new supporting material, can adsorb 59.58% of DD-PA. The BET showed the pore structure was changed and the DD-PA was adsorbed into the holes of HPMC. DD-PA distributed uniformly in the pore of HPMC by physical interaction. The melting and solidifying peak phase change temperature of DD-PA/HPMC was 19.34 °C and 15.92 °C, and the melting and solidifying latent heat was 113.12 J g⁻¹ and 94.47 J g⁻¹. Thermal cycling test exhibited that the melting peak phase change temperature and latent heat changed -4.29% and -1.02%, after 100 times cycling. The TG showed that the DD-PA/HPMC owned favorable thermal stability in working temperature. The 2% MW CNTs increased 32.30% thermal conductivity. The thermal storage and release rate rose clearly with the MW CNTs loading.

Acknowledgements This work was financially supported by Guangdong Basic and Applied Basic Research Foundation (2020A1515011411), Key Research special Projects in Universities in Guangdong Province (2019KZDZX2002), the National Natural Science Foundation of China (31570572), and Guangzhou Science and Technology Project (201905010005) and the Project of Key Disciplines of Forestry Engineering of Bureau of Guangzhou Municipality.

References

- Xu Y, Li MJ, Zheng ZJ, Xue XD. Melting performance enhancement of phase change material by a limited amount of metal foam: Configurational optimization and economic assessment. *Appl Energ*. 2018;212:868–80.
- Yuan P, Zhang P, Liang T, Zhai SP, Yang DG. Effects of functionalization on energy storage properties and thermal conductivity of graphene/*n*-octadecane composite phase change materials. *J Mater Sci*. 2019;54(2):1488–501.
- Masoumi H, Khoshkhoo RH, Mirfendereski SM. Modification of physical and thermal characteristics of stearic acid as a phase change materials using TiO₂-nanoparticles. *Thermochim Acta*. 2019;675:9–17.
- Sheng N, Dong KX, Zhu CY, Akiyama T, Nomura T. Thermal conductivity enhancement of erythritol phase change material with percolated aluminum filler. *Mater Chem Phys*. 2019;229:87–91.
- Tang YJ, Jia YT, Alva G, Huang X, Fang GY. Synthesis, characterization and properties of palmitic acid/high density polyethylene/graphene nanoplatelets composites as form-stable phase change materials. *Sol Energy Mat Sol C*. 2016;155:421–9.
- Tang BT, Wu C, Qiu MG, Zhang XW, Zhang SF. PEG/SiO₂-Al₂O₃ hybrid form-stable phase change materials with enhanced thermal conductivity. *Mater Chem Phys*. 2014;144(1–2):162–7.
- Peng SQ, Huang J, Wang TY, Zhu PP. Effect of fumed silica additive on supercooling thermal reliability and thermal stability of Na₂HPO₄ center dot 12H₂O as inorganic PCM. *Thermochim Acta*. 2019;675:1–8.
- Temel UN, Kurtulus S, Parlak M, Yapici K. Size-dependent thermal properties of multi-walled carbon nanotubes embedded in phase change materials. *J Therm Anal Calorim*. 2018;132:631–41.
- Wang W, Wang CY, Wang T, Li W, Chen LJ, Zou RG, Zheng J, Li XG. Enhancing the thermal conductivity of *n*-eicosane/silica phase change materials by reduced graphene oxide. *Mater Chem Phys*. 2014;147(3):701–6.
- Qian YC, Zhang Y, Sun JH, Song C, Jing Y, Shao F, Jia YZ, Tao ZY, Wang XQ, Liu H. The effect of hydrophilic modification of expanded graphite on the thermophysical properties of magnesium chloride hexahydrate. *J Therm Anal Calorim*. 2019. <https://doi.org/10.1007/s10973-019-08942-x>.
- Hohlein S, Konig-Haagen A, Bruggemann D. Thermophysical Characterization of MgCl₂ center dot 6H₂O, Xylitol and Erythritol as Phase Change Materials (PCM) for Latent Heat Thermal Energy Storage (LHTES). *Materials*. 2017;10(4):444. <https://doi.org/10.3390/ma10040444>.
- Wu B, Zhao Y, Liu Q, Zhou CL, Zhang X, Lei JX. Form-stable phase change materials based on castor oil and palmitic acid for renewable thermal energy storage. *J Therm Anal Calorim*. 2019;137:1225–32.
- Han LP, Ma GX, Xie SL, Sun JH, Jia YZ, Jing Y. Preparation and characterization of the shape-stabilized phase change material based on sebacic acid and mesoporous MCM-41. *J Therm Anal Calorim*. 2017;130:935–41.
- Ramakrishnan S, Wang XM, Sanjayan J. Thermal enhancement of paraffin/hydrophobic expanded perlite granular phase change composite using graphene nanoplatelets. *Energ Buildings*. 2018;169:206–15.
- Cheng XM, Li G, Yu GM, Li YY, Han JQ. Effect of expanded graphite and carbon nanotubes on the thermal performance of stearic acid phase change materials. *J Mater Sci*. 2017;52(20):12370–9.
- Ziapour BM, Hashtroudi A. Performance study of an enhanced solar greenhouse combined with the phase change material using genetic algorithm optimization method. *Appl Therm Eng*. 2017;110:253–64.
- Lee KO, Medina MA, Sun XQ, Jin X. Thermal performance of phase change materials (PCM)-enhanced cellulose insulation in passive solar residential building walls. *Sol Energy*. 2018;163:113–21.
- Chalco-Sandoval W, Fabra MJ, Lopez-Rubio A, Lagaron JM. Use of phase change materials to develop electrospun coatings of interest in food packaging applications. *J Food Eng*. 2017;192:122–8.
- Cheng WL, Mei BJ, Liu YN, Huang YH, Yuan XD. A novel household refrigerator with shape-stabilized PCM (Phase Change Material) heat storage condensers: An experimental investigation. *Energy*. 2011;36(10):5797–804.
- Wu B, Fu WX, Kong BW, Hu K, Zhou CL, Lei JX. Preparation and characterization of stearic acid/polyurethane composites as dual phase change material for thermal energy storage. *J Therm Anal Calorim*. 2018;132:907–17.
- Sari A, Karaipekli A, Alkan C. Preparation, characterization and thermal properties of lauric acid/expanded perlite as novel form-stable composite phase change material. *Chem Eng J*. 2009;155(3):899–904.
- Zhang D, Zhou HM, Wu K, Li ZJ. Granular phase changing composites for thermal energy storage. *Sol Energy*. 2005;78(3):471–80.

23. Karaipekli A, Sari A. Capric-myristic acid/expanded perlite composite as form-stable phase change material for latent heat thermal energy storage. *Renew Energ.* 2008;33(12):2599–605.
24. Zhu N, Liu PP, Liu FL, Hu PF, Wu MD. Energy performance of double shape-stabilized phase change materials wallboards in office building. *Appl Therm Eng.* 2016;105:180–8.
25. Delcroix B, Kummert M, Daoud A. Development and numerical validation of a new model for walls with phase change materials implemented in TRNSYS. *J Build Perform Simu.* 2017;10(4):422–37.
26. Xia Y, Zhang XS. Experimental research on a double-layer radiant floor system with phase change material under heating mode. *Appl Therm Eng.* 2016;96:600–6.
27. Xia YP, Cui WW, Zhang HZ, Zou YJ, Xiang CL, Chu HL, Qiu SJ, Xu F, Sun LX. Preparation and thermal performance of n-octadecane/expanded graphite composite phase-change materials for thermal management. *J Therm Anal Calorim.* 2018;131:81–8.
28. Kumar R, Vyas S, Dixit A. Fatty acids/1-dodecanol binary eutectic phase change materials for low temperature solar thermal applications: Design, development and thermal analysis. *Sol Energy.* 2017;155:1373–9.
29. Konuklu Y, Paksoy HO, Unal M, Konuklu S. Microencapsulation of a fatty acid with Poly (melamine-urea-formaldehyde). *Energy Convers Manage.* 2014;80:382–90.
30. Huang JY, Lu SL, Kong XF, Liu SB, Li YR. Form-stable phase change materials based on eutectic mixture of tetradecanol and fatty acids for building energy storage: preparation and performance analysis. *Materials.* 2013;6(10):4758–75.
31. Yang XJ, Yuan YP, Zhang N, Cao XL, Liu C. Preparation and properties of myristic-palmitic-stearic acid/expanded graphite composites as phase change materials for energy storage. *Sol Energy.* 2014;99:259–66.
32. Liang K, Shi L, Zhang JY, Cheng J, Wang XD. Fabrication of shape-stable composite phase change materials based on lauric acid and graphene/graphene oxide complex aerogels for enhancement of thermal energy storage and electrical conduction. *Thermochim Acta.* 2018;664:1–15.
33. Sobolciak P, Karkri M, Al-Maaded MA, Krupa I. Thermal characterization of phase change materials based on linear low-density polyethylene, paraffin wax and expanded graphite. *Renew Energ.* 2016;88:372–82.
34. Zhang N, Yuan YP, Yuan YG, Cao XL, Yang XJ. Effect of carbon nanotubes on the thermal behavior of palmitic-stearic acid eutectic mixtures as phase change materials for energy storage. *Sol Energy.* 2014;110:64–70.
35. Han ZD, Fina A. Thermal conductivity of carbon nanotubes and their polymer nanocomposites: a review. *Prog Polym Sci.* 2011;36(7):914–44.
36. Xu BW, Li ZJ. Paraffin/diatomite/multi-wall carbon nanotubes composite phase change material tailor-made for thermal energy storage cement-based composites. *Energy.* 2014;72:371–80.
37. Mitran RA, Berger D, Munteanu C, Matei C. Evaluation of different mesoporous silica supports for energy storage in shape-stabilized phase change materials with dual thermal responses. *J Phys Chem C.* 2015;119(27):15177–84.
38. Madani SH, Hu C, Silvestre-Albero A, Biggs MJ, Rodriguez-Reinoso F, Pendleton P. Pore size distributions derived from adsorption isotherms, immersion calorimetry, and isosteric heats: a comparative study. *Carbon.* 2016;96:1106–13.
39. Radhakrishnan R, Gubbins KE. Free energy studies of freezing in slit pores: an order-parameter approach using Monte Carlo simulation. *Mol Phys.* 1999;96(8):1249–67.
40. Li TX, Lee JH, Wang RZ, Kang YT. Enhancement of heat transfer for thermal energy storage application using stearic acid nanocomposite with multi-walled carbon nanotubes. *Energy.* 2013;55:752–61.

Publisher's Note Springer Nature remains neutral with regard to jurisdictional claims in published maps and institutional affiliations.